Model Calibration of High Damping Rubber Bearings: A Preliminary Mass

Material Strength and Applied Mechanics
A. Khotsianovsky and Y. Chen (Eds.)

doi:10.3233/ATDE240571

Model Calibration of High Damping Rubber Bearings: A Preliminary Mass Production Reliability Study

Santiago LONDOÑO LÓPEZ. [a,1], Raffaele CUCUZZA [a]Majid MOVAHEDI RAD [b]
Marco DOMANESCHI [a] and Giuseppe Carlo MARANO [a]

[a] *Department of Structural, Geotechnical and Building Engineering. Politecnico di Torino, Torino, Italy*

[b] *Department of Structural and Geotechnical Engineering, Széchenyi István University, Gyor, Hungary.*

Abstract. Over the past decade, Building Isolation Systems (BIS) have gain significant relevance due to their ability to reduce horizontal acceleration and inter-story drifts in structures. Since the 1950s, researchers have focused on developing numerical models to simulate the dissipative behavior of High Damping Rubber Bearings (HDRB) in parallel major earthquake events have highlighted the need for BIS devices in medium and large-scale infrastructure, accentuating the need for further research into accurate models and adding the pressing interest in variability of mass-produced HDRB parameters. This study presents initial results from an identification process using two numerical models, validated using experimental tests at the SISMALAB laboratory. The experimental data involved eight samples subjected to compression forces and horizontal displacement. Optimal values were obtained through a Genetic Algorithm optimization process, minimizing discrepancies between experimental and numerical response. Preliminary variability analysis was conducted on data from 20 independent iterations over the eight samples.

Keywords. High Damper Rubber Bearings (HDRB), Numerical Model, Optimization, Genetic Algorithm, Statistical Analysis

1. Introduction

Civil Engineers meticulously design structures to enhance safety [1] and resilience [2,3], particularly against seismic events. Building Isolation Systems (BIS), like High Damping Rubber Bearings (HDRBs), have emerged as an effective solutions, absorbing and dissipating energy during ground motion therefore reducing seismic forces transmitted to structures[4]. Compared to other methods, HDRBs offer simultaneous energy dissipation and deformation capacity across various frequencies, enhancing structural performance. Their well-documented numerical performance, durability, and straightforward installation position the devices as a leading alternative to improve the behavior of the structures[5,6]. Evidence of this can be seen in the extensive research on laws such as

[1]Corresponding Author: Santiago Londoño Lopez, santiago.londono@polito.it

algebraic, transcendental, and differential models. These models, which strive to replicate complex hysteretic behavior[7], balance accuracy with computational demand and ultimately offer a solid understanding of the phenomena[8]. The acquired knowledge and advantages of these devices pose an increasing demand in the market and raise new challenges for the industry and the researchers, as now their behavior in numerical models must accurately describe the response and also be safely replicable considering the massive production effects, therefore leading to a statistical understanding of the device behavior. To attempt to fill this new gap this paper researches the variability of the laws' parameters of two different numerical models to reproduce the experimental behavior of a mass-production HDRB device. Based on the outcomes provided in previous research of one of the authors [9,10], a preliminary discussion has been provided to identify the most accurate numerical model.

2. Numerical Models

Several numerical models have been formulated to accurately represent the behavior of High Damping Rubber Bearings (HDRBs), as documented in the literature. These models are classified based on the type of mathematical formulation required to evaluate the output variable. The Jankowski and Bouc-Wen models were selected for further investigation, considering the following attributes of each.

First, Jankowski model is well-established, computationally efficient, and capable of accurately representing various physical effects associated with HDRB hysteretic behavior, making it an appropriate selection among the group of algebraic laws. Second, the Bouc-Wen model is widely used, extensively validated, and offers a comprehensive description of hysteresis while effectively capturing nonlinear behavior.

The parameters for both models will be adjusted by defining an objective function (or cost function) [11] to be minimized through an identification process using the well-known Genetic Algorithm (GA). The goal is to achieve a satisfactory level of accuracy between the experimental data and the calculated output variables of each model[12,13, 14]

2.1. Jankowski et al. Model - Law #1 [15]

Rubber properties are responsible for non-linear hysteretic behavior, Jankowski et al. in their article proposed a non-linear strain rate-dependent transcendent model for HDRB devices under a constant vertical load and stable temperature. The model simulates horizontal response force using a nonlinear elastic spring dashpot element.[16]

The mathematical formulation of the adopted numerical model is shown in Eq.(1):

$$F = F_1(x(t),\dot{x}(t)) + F_2(x(t),\dot{x}(t)) \qquad F = K(x(t),\dot{x}(t)) \cdot x(t) + C(x(t),\dot{x}(t)) \cdot \dot{x}(t) \quad (1)$$

In these formulas, as shown in Eqn.s (2)-(3), the shear stiffness (K) and damping coefficients (C) at a given time (t) are calculated based on the appropriate values of experimental deformation ($x(t)$) and velocity ($\dot{x}(t)$).[17]

$$K(x(t),\dot{x}(t)) = a_1 + a_2 x^2(t) + a_3 x^4(t) + \frac{a_4}{\cosh^2(a_5\dot{x}(t))} + \frac{a_6}{\cosh(a_7\dot{x}(t))\cosh(a_8 x(t))} \tag{2}$$

$$C(x(t),\dot{x}(t)) = \frac{a_9 + a_{10}x^2(t)}{\sqrt{a_{11}^2 + \dot{x}^2(t)}} \tag{3}$$

In the model, parameters a_i are determined numerically by fitting experimental data using the GA search. Specifically, a_1 sets the baseline stiffness level, with a_2 and a_3 adjusting for larger shear strains. Parameters a_4 and a_5 control stiffness near maximum displacements, while a_6 to a_8 modifies stiffness for lower amplitude movements. Lastly, a_9 to a_{11} adjust the damping to shape the hysteresis loops as needed.

2.2. Bouc Wen Model - Law #4 [18]

The Bouc-Wen hysteresis model is recognized for its simplicity and effectiveness in reproducing experimental results, making it a favorite among practitioners. Its robustness in both mathematical and physical aspects, along with strong agreement between experimental and numerical data, supports its use for representing the force output of HDRB devices [19]. The mathematical formulation of such a model is reported in Eq. (4):

$$F(t) = \alpha K_i x(t) + (1-\alpha) K_i z(t) \tag{4}$$

In this context, K_i represents the model's stiffness before yielding, α denotes the ratio of stiffness before and after yielding. $x(t)$ represents the experimental deformation and $z(t)$ characterizes the hysteretic response. [20].

$$\frac{dz}{dt} = A \cdot \frac{dx}{dt} - \left(\beta \cdot \left|\frac{dx}{dt}\right| \cdot z \cdot |z|^{\eta-1}\right) - \left(\gamma \cdot \frac{dx}{dt} \cdot |z|^{\eta}\right) \tag{5}$$

The hysteretic variable $z(t)$ is introduced by defining the differential component of the model as observed in Eq. (5). The parameter A influences initial stiffness, β controls hysteresis cycle amplitude and energy dissipation, γ regulates unloading curve linearity, and n facilitates smooth phase transitions.

3. Experimental Campaign

From 2021 to 2023, the SISMALB s.r.l. laboratory conducted an experimental survey on periodically developed devices. Randomly chosen samples from different manufacturing lots were tested to ensure compliance with the Italian national annex and government regulations before shipment. Over 160 elastomeric isolators from the ISI-S 600/208 P40 series were evaluated. The experiments used SISMALAB's ISOL 1000 apparatus, featuring a hydraulic cylinder with pressure transducer control. The horizontal displacement was regulated by a load cell or position transducer on the piston rod, managed by the Sisma-Control program. A load cell between the actuator and HDRB specimen and a transducer tracked cyclic forces. The system's autonomous hydraulic control allowed

real-time adjustment and data acquisition, following a sinusoidal displacement-time pattern. The laboratory test protocol adhered to UNI EN 15129-8.2.1.2.2 for testing Horizontal Characteristics under Cyclic Deformation (H.C.C). A constant vertical load of 6 MPa was applied, followed by three sinusoidal cycles at 0.5 Hz, reaching a deformation equal to 100% of the total active thickness.

4. Identification Procedure

This section presents the mathematical formulation for the optimization problem, introducing the objective function and design variables. Reliability in terms of accuracy and dispersion was assessed by performing 20 runs for each device and observing parameter variability across the subjects. The settings were retrieved referring to the research of Cucuzza et al.[9], for this device typology and research scope, a population size of 100 and 50 iterations gave satisfactory results.

4.1. Mathematical Formulation

The calibration process for the model parameters involves solving an unconstrained optimization problem. The objective function (OF) aims to minimize the difference between experimental input and numerical output. The design vector x consists of parameters framed by their respective lower and upper bounds, x_i^l and x_i^u. This process evaluates the accuracy of both models for each device in the series. Reported in Eq. (6) is the problem statement for the OF.

$$\textbf{Minimize} \quad W = f(\mathbf{x_i}), \quad i = 1, \ldots, n \quad \textbf{Subject to} \quad x_i^l \leq x_i \leq x_i^u \tag{6}$$

The vector x=$\{x_1, ..., x_j, ..., x_n\}$ contains real parameters determined by the chosen numerical model, and its size corresponds to the variables governing the constitutive law. x^l=$\{x_1^l, ..., x_j^l, ..., x_n^l\}$ and x^u=$\{x_1^u, ..., x_j^u, ..., x_n^u\}$ represent the lower and upper bounds of x. These limits restrict x within a feasible solution sub-domain, where its values range between x^l and x^u. For this research, a suitable OF has been defined in integral form as introduce in Eq. (7):

$$f(x) = \frac{1}{\sigma_{p_m}(t_{end} - t_{start})} \int_{t_{start}}^{t_{end}} abs(p_m - p_e(x))dt \tag{7}$$

The start and end time records, denoted by t_{start} and t_{end} respectively, $p_m(t)$ represents experimentally measured force and $p_e(t)$ denote the numerically estimated force. For the Bouc Wen differential law, the Matlab ODE45 function utilizing the Runge-Kutta method was employed to solve the ordinary differential equations (nonstiff). The fixed time step matched the sampling time step during laboratory tests. To ease the optimization process and prevent numerical noise from critical values, lower (x^l) and upper (x^u) bounds for each design variable were predetermined based on a sensitivity analysis. This strategy aims to reduce computational effort by narrowing the optimization problem search domain, facilitating an efficient exploration phase of the algorithm [21]. In Table

1, the single design variable of the optimization problem and the corresponding range variability are displayed for each law.

Table 1.: Lower and upper bounds of the models' parameters

Law	Parameter	Lower Bound (X_l)	Upper Bound (X_u)
Law #1	a_1 **[N/m]**	10^4	10^6
Jankowski	a_2 **[N/m^3]**	10^6	9×10^6
Model	a_3 **[N/m^5]**	10^6	9×10^6
	a_4 **[N/m]**	10^3	10^5
	a_5 **[s/m]**	10^3	10^4
	a_6 **[N/m]**	10^5	3.5×10^6
	a_7 **[s/m]**	0	10
	a_8 **[1/m]**	5	20
	a_9 **[N]**	10^4	10^5
	a_{10} **[N/m^2]**	10^4	10^5
	a_{11} **[m/s]**	0	10
Law #2	α **[-]**	0.1	0.2
BoucWen	Ke **[kN/mm]**	2	4
Model	A **[-]**	1	2
	β **[1/mm]**	0.025	0.075
	n **[-]**	1	1.25
	γ **[1/mm]**	0.025	0.075

5. Statistical Analysis

The results obtained through the optimization for both numerical models will be introduced, and some visual representation will detail the significance of the findings.

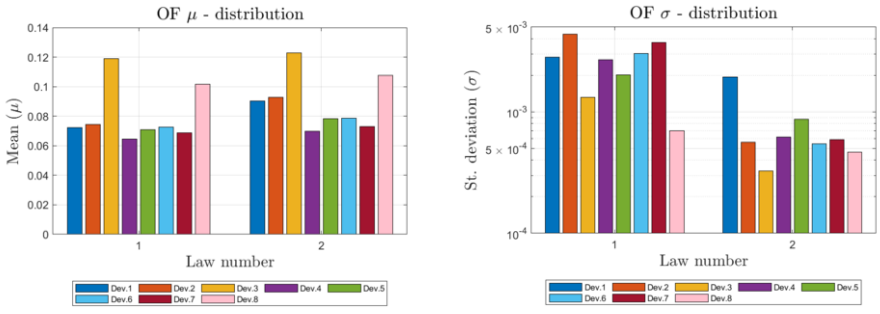

(a) (b)

Figure 1. OF mean (μ) distribution for each test devices (a); OF standard deviation (σ) distribution for each test devices (b). For each law, ($X - axis$), a color legend is assigned to each device

Figure 1 presents a bar representation of the mean (μ) and standard deviation (σ) distribution for both hysteresis models, including the 8 sampled devices and consider-

ing the 20 runs for each device. Particularly, Fig. 1(a) depicts, in terms of OF, the accuracy of each device to properly fit the experimental data. Closing in, is possible to determine in both Laws an approximate error of around 8%, with a slightly better mean precision for Jandowski model (Law#1). In terms of overall dispersion, Fig. 1(b) tilts the crossing found between both models, as the precision for both were relatively the same, the dispersion after performing 20 iterations in the parameters calibration showed that BoucWen Model is more robust and sufficiently accurate for the data at hand. After reviewing the overall behavior, a device-by-device accuracy review considering both models under study is presented in Fig. 1(a). In terms of expected behavior, is worth mentioning that disregarding the model, the devices behave similarly. Being the most accurate in both laws devices #4, #5, #6 and #7 and the worst performers devices #3 and #8.

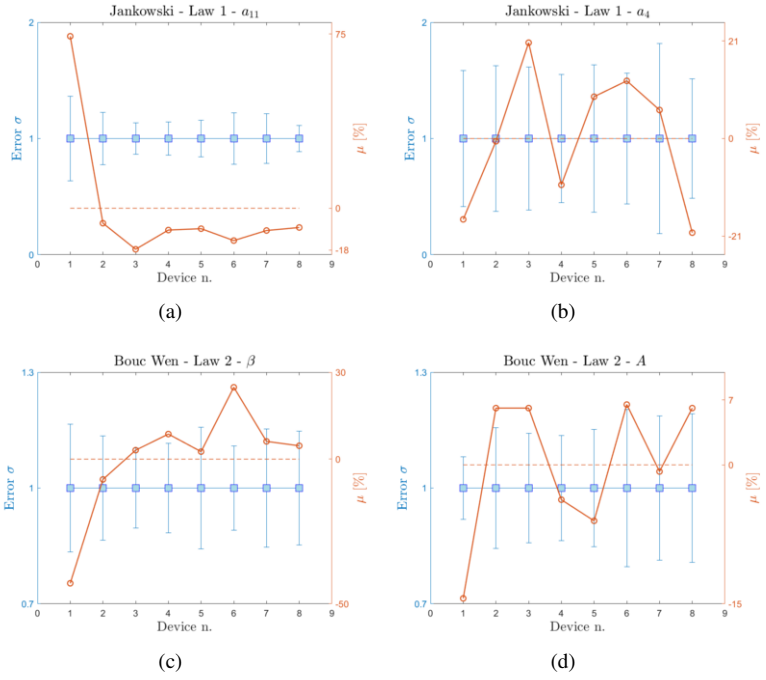

Figure 2. Normalized standard deviation and mean distribution of the identified a_{11} (a), a_4 (b) for law #1 and β (c), A (d) for law #2.. The left $y-axis$ shows the standard deviation error bar (σ), while the right $y-axis$ is the percentage variation of mean distribution (μ). The dotted line represents the mean reference value among all ten mean values calculated over 20 runs for each device.

A follow-up question related to calibration and the statistical results is the influence of each calibrated parameter on the overall accuracy and dispersion of the model. After addressing each parameter for both models, the most significant outliers in accuracy and precision are introduced in Fig. 2. It displays graphs with two vertical axes: on the left side, it shows the standard deviation of the parameter relative to the mean of all runs for each device (represented by error bars denoting the standard deviation, $Error\ \sigma$). Meanwhile, the right axis illustrates the percentage variation of the parameter's mean (calculated over 20 optimization runs) compared to the reference mean value. The reference

mean value, shown as a red dotted line, is determined as the mean of all mean values for each device.

For Jankowski model, Fig. 2(a) displays a dominant mean error in the parameter a_{11} for device 1, overcoming the mean at about 75%. This result is particularly interesting since within the numerical formulation of Jankowski's equation, this parameter controls the energy dissipation and degradation. In terms of the parameter that shows the largest dispersion Fig. 2(b) indicates a μ error of about 1.5 for parameter a_4, being an almost constant trend for all devices. According to Jankowski's approach the largest even dispersion among all devices for calibrating a_4 might represent inconsistencies to fit a value regarding the stiffness for maximum displacements. The Bouc-Wen model parameters represented in Fig. 2(c) show, in terms of μ, a peak discrepancy of 80% in parameter β with respect to the reference average value, being particularly prominent for device 1, in which a value of about 50% error with respect to the average is identified. The model attributes this parameter to the control of the energy dissipation and the amplitude of the hysteresis cycle. For the same law, referring to the dispersion (Fig.2(d)), parameter A is a slightly above the average dispersion, encountering a maximum value of around 1.25.The physical meaning given by Bouc-Wen to this parameter relates to the setting of the initial stiffness. The variability related to the fixing of such a parameter will be further discussed in the upcoming section.

6. Closing Remarks and Future Developments

As shown in Fig. 3, a satisfactory fit between the selected numerical models and the experimental data has been achieved. The results from the independent runs using the genetic algorithm (GA) indicate a mean average error of approximately 8% for the Jankowski model and around 9% for the Bouc-Wen model (see Fig. 4). The experimental test used for this calibration, as described in UNI EN 15129-8.2.1.2.2 for testing Horizontal Characteristics under Cyclic Deformation (H.C.C.), does not allow for the visualization of large progressive deformations. Consequently, effects such as aging, pinching, and stiffness degradation were not observable, either for the evolutionary algorithm or for the numerical models.

Given this limitation, it is important to note that practitioners intending to use this procedure for calibrating and selecting the appropriate numerical model must also take into account the intended performance of the device. Specifically, for this particular set of data, the HDRBs were not subjected to deformations beyond their elastic range, and the fitting of the models is directly related to this condition. Therefore, if a model is required in the F.E. software to compute the base response and perform verifications for large deformations, the HDRB numerical model used to compute the horizontal force might not be suitable for elastoplastic deformations or when degradation is considered. Since the experimental data were only tested and calibrated within the elastic range, the selected model may not perform optimally for other conditions.

Finally, a the future attempt to correlate in a deeper way the physical meaning of a given parameter's accuracy lost or massive dispersion might be of interest. Particularly if such analysis might lead to identifying a production lot of devices with manufacturing issues or out-of-trend response. Preliminarily, in accordance with the results obtained in Fig. 2. The lot where Device 1 was subtracted might have out range rubber mixture since param-

eters of the models regarding energy dissipation and initial stiffness are inconsistent and out of trend. However, such an assumption requires further study. The future research goals will initially consider to increase the number and typology of models, using two or three typologies of each category (e.g algebraic, transcendent and differential), also, increase the number of devices to explore furthermore the production variability, including, if possible, results from other laboratories, over devices from other production factories. Using these measures seeks to improve the OF error, to outperform the calibration for this test typology in terms of accuracy and robustness. Such ideas are possible due to the vast experimental data available and the computational resources at the disposal to perform several iterations using the G.A.

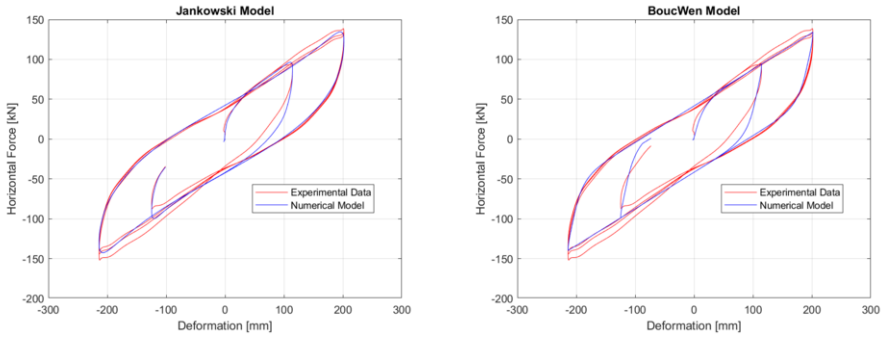

(a) (b)

Figure 3. Comparison between experimental and numerical force-displacement relationships for the algebraic and differential models (refers respectively to law #1 (a), law#2 (b)) with specific regard to Device #4 Test #20

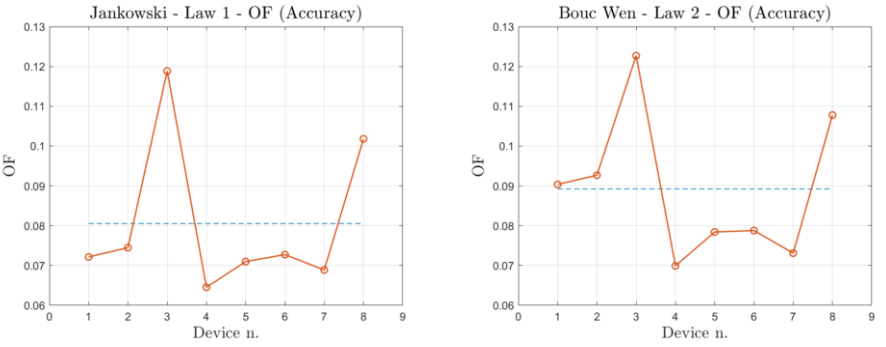

(a) (b)

Figure 4. OF mean (μ) values for each device considering 20 independent runs for each device and each law. The dotted line represents the mean values calculated over the 8 devices.

References

[1] Cucuzza R, Aloisio A, M M, Domaneschi M. Constructability-based Optimization for Steel Structures: From Truss Beams to Large-Scale Industrial Buildings (approaching final Editor decision). Automation in Construction. 2024.

[2] Domaneschi M, Cucuzza R. Structural Resilience through Structural Health Monitoring: A Critical Review. Data Driven Methods for Civil Structural Health Monitoring and Resilience. 2024:1-13.

[3] Domaneschi M, Cucuzza R, Martinelli L, Noori M, Marano GC. A probabilistic framework for the resilience assessment of transport infrastructure systems via structural health monitoring and control based on a cost function approach. Structure and Infrastructure Engineering. 2024:1-13.

[4] Kelly JM. Earthquake-resistant design with rubber. vol. 7. Springer; 1993.

[5] Gu Z, Lei Y, Qian W, Xiang Z, Hao F, Wang Y. An experimental study on the mechanical properties of a high damping rubber bearing with low shape factor. Applied Sciences. 2021;11(21):10059.

[6] Cucuzza R, Domaneschi M, Camata G, Marano GC, Formisano A, Brigante D. FRCM retrofitting techniques for masonry walls: A literature review and some laboratory tests. Procedia Structural Integrity. 2023;44:2190-7.

[7] Sadeghpour A, Ozay G. Calculating the collapse margin ratio of RC frames using soft computing models. Structural Engineering and Mechanics, An Int'l Journal. 2022;83(3):327-40.

[8] Capuano R, Fraddosio A, Piccioni MD. Phenomenological rate-independent uniaxial hysteretic models: A mini-review. Frontiers in Built Environment. 2022;8:1048533.

[9] Cucuzza R, Domaneschi M, Greco R, Marano GC. Numerical models comparison for fluid-viscous dampers: Performance investigations through Genetic Algorithm. Computers and Structures. 2023;288.

[10] Olivo J, Cucuzza R, Bertagnoli G, Domaneschi M. Optimal design of steel exoskeleton for the retrofitting of RC buildings via genetic algorithm. Computers & Structures. 2024;299:107396.

[11] Cucuzza R, Aloisio A, Domaneschi M, Nascimbene R. Multimodal seismic assessment of infrastructures retrofitted with exoskeletons: insights from the Foggia Airport case study. Bulletin of Earthquake Engineering. 2024:1-29.

[12] Quaranta G, Marano GC, Greco R, Monti G. Parametric identification of seismic isolators using differential evolution and particle swarm optimization. Applied Soft Computing Journal. 2014;22:458-64. Available from: https://www.scopus.com/inward/record.uri?eid=2-s2.0-84903738365&doi=10.1016%2fj.asoc.2014.04.039&partnerID=40&md5=f3dca21b3e938909a12e8da41f1da5d2.

[13] Marano GC, Quaranta G, Monti G. Modified Genetic Algorithm for the Dynamic Identification of Structural Systems Using Incomplete Measurements. Computer-Aided Civil and Infrastructure Engineering. 2011;26(2):92-110. Available from: https://www.scopus.com/inward/record.uri?eid=2-s2.0-78651435257&doi=10.1111%2fj.1467-8667.2010.00659.x&partnerID=40&md5=655d045ec2a46f7aad438178878d58c6.

[14] Marano GC, Quaranta G, Avakian J, Palmeri A. Identification of Passive Devices for Vibration Control by Evolutionary Algorithms; 2013. Available from: https://www.scopus.com/inward/record.uri?eid=2-s2.0-84882603167&doi=10.1016%2fB978-0-12-398364-0.00015-2&partnerID=40&md5=0be21dc5e85f48e7fb8375249dfc60aa.

[15] Jankowski J. A Non-Linear Approach to Data Analysis. In: Proceedings of the 13th World Conference on Earthquake Engineering. Vancouver, B.C., Canada; 2004. Paper No. 1897.

[16] Jankowski R, Wilde K, Fujino Y. Reduction of pounding effects in elevated bridges during earthquakes. Earthquake engineering & structural dynamics. 2000;29(2):195-212.

[17] Jankowski R. Nonlinear rate dependent model of high damping rubber bearing. Bulletin of Earthquake Engineering. 2003;1:397-403.

[18] Bouc R. Forced vibrations of mechanical systems with hysteresis. In: Proc. of the Fourth Conference on Nonlinear Oscillations, Prague, 1967; 1967. .

[19] Ismail M, Ikhouane F, Rodellar J. The hysteresis Bouc-Wen model, a survey. Archives of Computational Methods in Engineering. 2009;16(2):161-88. Cited By 557.

[20] Domaneschi M. Simulation of controlled hysteresis by the semi-active Bouc-Wen model. Computers and Structures. 2012;106-107:245-57. Cited By 43.

[21] Habashneh M, Cucuzza R, Domaneschi M, Rad MM. Advanced elasto-plastic topology optimization of steel beams under elevated temperatures. Advances in Engineering Software. 2024;190:103596.